



Joint multi-parameter optical performance monitoring scheme based on trajectory information for a Stokes vector direct detection system

XINKUO YU,^{1,2} CHENGLIN BAI,^{1,2,4} LISHAN YANG,^{1,2} HENGYING XU,^{1,2,5} WEIBIN SUN,^{1,2} AND JIAPING LI³

¹School of Physics Science and Information Engineering, Liaocheng University, Liaocheng 252000, China

²Shandong Provincial Key Laboratory of Optical Communication Science and Technology, Liaocheng 252000, China

³Institute of Advanced Photonics Technology, School of Information Engineering, and Guangdong Provincial Key Laboratory of Information Photonics Technology, Guangdong University of Technology, Guangzhou 510006, China

⁴e-mail: baichenglin@lcu.edu.cn

⁵e-mail: xuhengying@qq.com

Received 25 November 2021; revised 23 January 2022; accepted 24 January 2022; posted 25 January 2022; published 22 February 2022

In this study, we propose and verify a joint multi-parameter optical performance monitoring (OPM) scheme based on trajectory information for the Stokes vector direct detection (SVDD) system, for the first time, to the best of our knowledge. Here, the proposed scheme first performs quantification of the trajectory to construct trajectory information, which not only presents diversity of the received symbols in spatial dimension, but also records the jump pattern among symbols in time dimension. Subsequently, eigenanalysis is introduced to extract critical features hidden in trajectory information and simultaneously achieve the purpose of dimensionality reduction. The effectiveness of the scheme is verified through 14/28 Gbaud SVDD binary phase shift keying/quadrature phase shift keying/-8 quadrature amplitude modulation (QAM)/-16QAM/-32QAM/-64QAM simulation systems. Under the scenario of joint modulation format (MF) identification and optical signal to noise ratio (OSNR) monitoring, the identification rates of all six kinds of MFs achieve 100% within their corresponding reasonable OSNR ranges. Besides that, the average mean absolute error (MAE) of the monitored OSNRs are obtained as 0.03 dB, 0.22 dB, 0.36 dB, 0.41 dB, 0.46 dB, and 0.49 dB for those six kinds of MFs, respectively. Under the scenario of multi-parameter OPM, SVDD-8QAM/-16QAM/-32QAM signals are 100% successfully identified when residual chromatic dispersion (RCD) is located in the ranges of 0–200 ps/nm, 0–190 ps/nm, and 0–160 ps/nm, respectively. The average MAE of OSNR monitoring and RCD estimation for these three commonly used MFs are 1.08 dB and 3.23 ps/nm, respectively. Moreover, the study also demonstrates the robustness for baud rates and a relatively simpler calculation complexity about the proposed OPM scheme. © 2022 Optica Publishing Group

<https://doi.org/10.1364/AO.449392>

1. INTRODUCTION

With the broad applications of 5G, internet of things, and cloud computing, short-reach optical communications are moving towards low-redundancy and low-power consumption to cope with the increasing demand for capacity [1]. Compared with the long-haul backbone optical network, the short-reach optical network requires us to deploy vast transceivers to connect diverse areas [2]. Therefore, the cost, system complexity, and spectral efficiency (SE) are referred to as the key considerations. Transponders for the short-reach optical network should rely on direct detection (DD), i.e., self-beating, rather than coherent detection to meet the requirements regarding cost,

size, and power consumption [3]. However, traditional intensity modulation-DD (IM-DD) schemes often use one degree of freedom of lightwaves, i.e., amplitude, resulting in relatively lower SE. In 2014, Che *et al.* reported a Stokes vector DD (SVDD) scheme for short-reach optical communication, which used two degrees of freedom, including the amplitude and phase of lightwaves, to achieve the same SE values as that of the single-polarization coherent detection [4]. In those studies, the results of SVDD were endowed with low system complexity since it did not require a local oscillator (LO) laser and had natural immunity to frequency offset and phase noise. Therefore, the

application of SVDD is generally considered one of the promising solutions for short-reach optical communications. Recently, various digital signal processing (DSP) technologies have been specially devised for SVDD, including polarization demultiplexing, equalizer for rotation of state-of-polarization (RSOP), chromatic dispersion (CD) compensation, etc. [5–7].

In further applications of complex network structures and scarce spectrum resources, essential principles have been proposed to monitor various network performance parameters, with the purpose of optimizing resource utilization and allocating a just-enough system margin [8,9]. In the last few years, various interesting optical performance monitoring (OPM) schemes have been reported. Among them, researchers designed various methods to achieve customized monitoring for a single parameter, such as Stokes space-based technology [10–12], machine learning-based technology [13–17], particle swarm optimization-based technology [18,19], data aided-based technology [20,21], statistical theory-based technology [22–24], and delay-tap-sampling-based technology [25]. Furthermore, various joint multi-parameter monitoring schemes have been developed recently, including machine learning-based technology [26–32], statistical theory-based technology [33,34], clustering-based technology [35], Godard's error-based technology [36], and Kalman filter-based technology [7]. All of those schemes have demonstrated effective results, whereas these approaches are still behind one's expectations in studies on short-reach optical communications, showing certain issues, such as achieving only a single function and needing a significant mass of training samples, which may cause higher computational complexity and cause a dilemma on previous computing resources.

In this paper, we propose a simplified joint multi-parameter monitoring scheme based on the trajectory information of received signals for the SVDD system. It can simultaneously realize the joint modulation format identification (MFI), optical signal-to-noise ratio (OSNR) monitoring, and residual CD (RCD) estimation. To the best of our knowledge, it seems that the study on trajectory information of received signals has not been reported to carry out OPM in short-reach optical communications. In our proposed scheme, first, the trajectory information of received signals is to be qualified. Then, an eigenanalysis is utilized to extract the critical features contained in the trajectory information for the purpose of dimensionality reduction. After that, the operations of joint multi-parameter OPMs are carried out for the SVDD system. The effectiveness of the proposed scheme has been verified by 14/28 Gbaud SVDD binary phase shift keying (BPSK)/quadrature phase shift keying (QPSK)/-8 quadrature amplitude modulation (QAM)/-16QAM/-32QAM/-64QAM simulation systems.

The rest of this paper is organized as follows: first, detailed operation principles of the proposed OPM scheme are demonstrated in Section 2. Then, the simulation setting and results are described in Section 3. Afterwards, the performance of the proposed scheme is further studied to verify its robustness for baud rate and computational complexity in Section 4. Finally, the conclusion is made in Section 5.

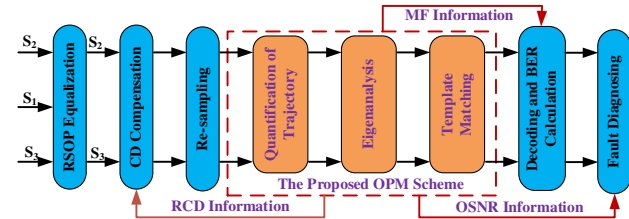


Fig. 1. DSP module architecture of the SVDD system.

2. OPERATING PRINCIPLES

In order to recover the transmitting information correctly, a DSP module is employed behind the Stokes vector receiver (SVR), which is illustrated in Fig. 1. First, the digital signals $S' = [S'_1, S'_2, S'_3]^T$ are obtained via the SVR. Then, the least-mean square (LMS)-based blind equalization algorithm is carried out in Stokes space to eliminate the RSOP effect [5,6]. After that, CD compensation is performed based on CD scanning and the frequency domain equalizer [37]. It should be noted that certain RCDs deteriorate the signal quality, which is closely related to the step size of CD scanning. After resampling, the proposed scheme is implemented based on trajectory information. The proposed scheme can be further split into three stages, including quantification of trajectory, eigenanalysis, and template matching. Finally, the identified MF information will be fed into the decoding module to de-modulate signal accurately and calculate bit error rates (BER). Moreover, the estimated RCD information can be fed back to the CD compensation module to improve its accuracy, and the obtained OSNR information is utilized to perform fault diagnoses. The proposed OPM scheme would be described in the following contents.

A. Quantification of Trajectory

First, the S_2 and S_3 components are normalized after resampling, and then they performed a folding operation by modulus calculation to assure that the values are all within the range of $[0,1]$. It is worth noting that the gains brought by the folding operation will be discussed in Section 3.B. Subsequently, a uniform mesh is designed by dividing the quadrate region with the range of $[0,1]$ into $M * M$ individual cells. Inspired by the discrete-time Markov chain (DTMC) [38], each individual cell is referred to as a state among the state space and is tagged from one to $M * M$, where M signifies the mesh density. Afterwards, each symbol is attached with the corresponding state label in light of its position within the quadrate area. With that, starting from the first status corresponding to the first symbol, the adjacent states are connected with lines until the state corresponding to the last symbol ends, and the quantity of line drawings between any two states is called weighting coefficients. Finally, all weighting coefficients calculated are used to construct the weight coefficient matrix \mathbf{A} to complete the quantification of trajectory. In detail, A_{ij} is the weight coefficient between state i and state j , and it should be noted that the weight coefficient matrix \mathbf{A} is a Hermitian matrix. Taking the received SVDD-16QAM symbols up to 8192 under OSNR of 33 dB serially as an example, the quantification process of the trajectory with the aid of a uniform mesh is exhibited in Fig. 2. Among them, Fig. 2(a) is a scatter plot of normalized S_2 and S_3

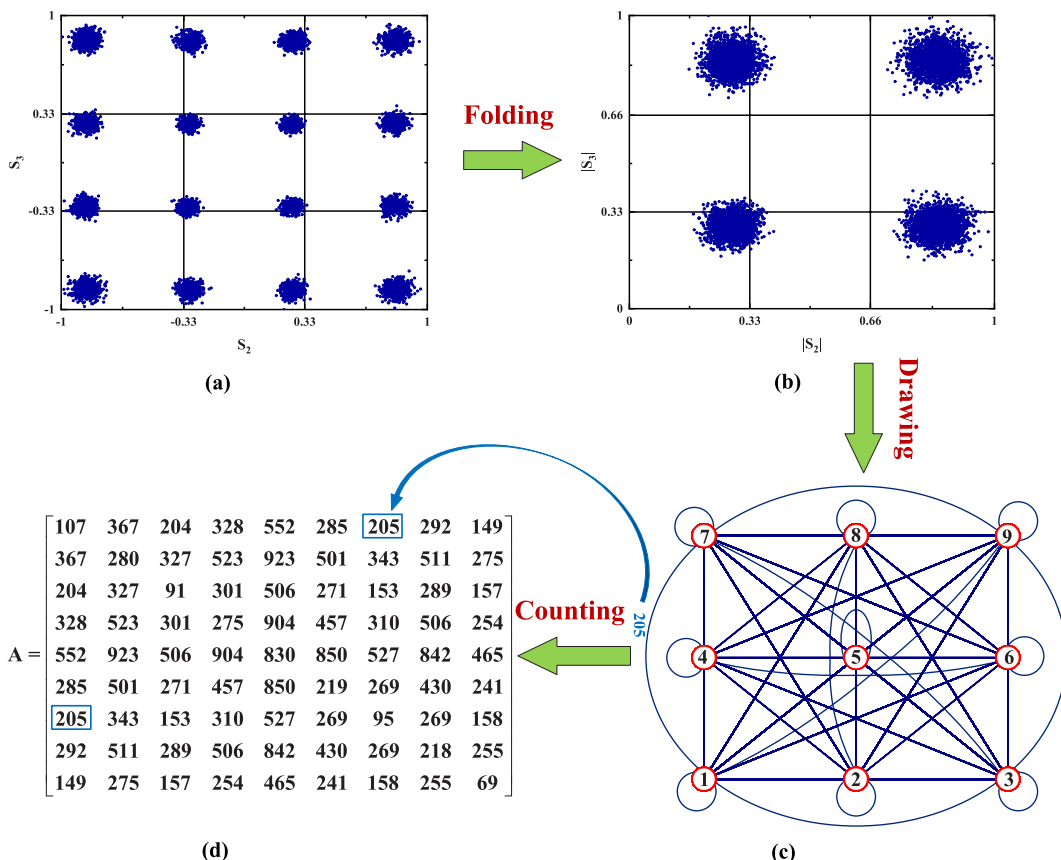


Fig. 2. Quantification process of the trajectory with the aid of a uniform mesh. (a) Scatter plot after normalization, (b) scatter plot after folding, (c) trajectory describing the jump pattern between different states, and (d) the weight coefficient matrix for the received 8192 SVDD-16QAM symbols under OSNR of 33 dB.

components, and Fig. 2(b) is a scatter plot with a uniform mesh after performing the folding operation by calculating moduli for S_2 and S_3 components, where the mesh density M is set to three. Figure 2(c) displays the trajectory describing the jump pattern between different states. The weight coefficient matrix \mathbf{A} is obtained by calculating the number of jumps between different states, as shown in Fig. 2(d). For instance, the number of jumps between state 1 and state 7 is 205, so the element $A_{17} = A_{71} = 205$ of the weight coefficient matrix \mathbf{A} .

B. Eigenanalysis

In pattern recognition, the primordial matrix data needs to be transformed or processed into a low-dimensional vector. Since it is a critical feature extracted from the primitive data and directly used for pattern clustering and classification, the low-dimensional vector is named an eigenvector. Given that eigenanalysis has been diffusely applied in mathematics and engineering [39], in this study, we intend to utilize eigenanalysis to extract the critical features hidden in the Hermitian matrix and to achieve the purpose of dimensionality reduction simultaneously. The expression of the eigenvalue issue of linear transformation can be written as

$$\mathbf{A}\mathbf{u} = \lambda\mathbf{u}, \quad \mathbf{u} \neq \mathbf{0}, \quad (1)$$

where \mathbf{A} represents the standard matrix of linear transformation, scalar λ denotes the eigenvalue of matrix \mathbf{A} , and vector \mathbf{u} is the eigenvector corresponding to λ . Given that all eigenvalues are real, the Hermitian matrix $\mathbf{A} \in \mathbb{C}^{n \times n}$ can be decomposed as follows:

$$\mathbf{A} = \mathbf{U} \sum \mathbf{U}^H, \quad (2)$$

where H denotes the conjugate transpose operator, $\sum = \text{diag}\{\lambda_1, \lambda_2, \dots, \lambda_N\}$ is a diagonal matrix of eigenvalues ordering as $\lambda_1 \leq \lambda_2 \leq \dots \leq \lambda_N$, which is called the spectral of matrix $\mathbf{A} \in \mathbb{C}^{n \times n}$, and its corresponding eigenvectors constitutes the eigenvector matrix $\mathbf{U} = \{\mathbf{u}_1, \mathbf{u}_2, \dots, \mathbf{u}_N\}$. Under these experimental conditions, the largest eigenvalue λ_{\max} is defined as the spectral radius, and its corresponding eigenvector \mathbf{u}_{\max} , which reflects the key feature, can be regarded as an ingenious option to carry out OPM.

C. Template Matching

Regarding the pattern classification aspect, it is assumed that there are M types of pattern vectors $\mathbf{s}_1, \mathbf{s}_2, \dots, \mathbf{s}_M$. Through a similarity measurement, the unknown pattern vectors \mathbf{x} need to be compared with M known pattern vectors to determine which category it belongs to. In addition to distance function,

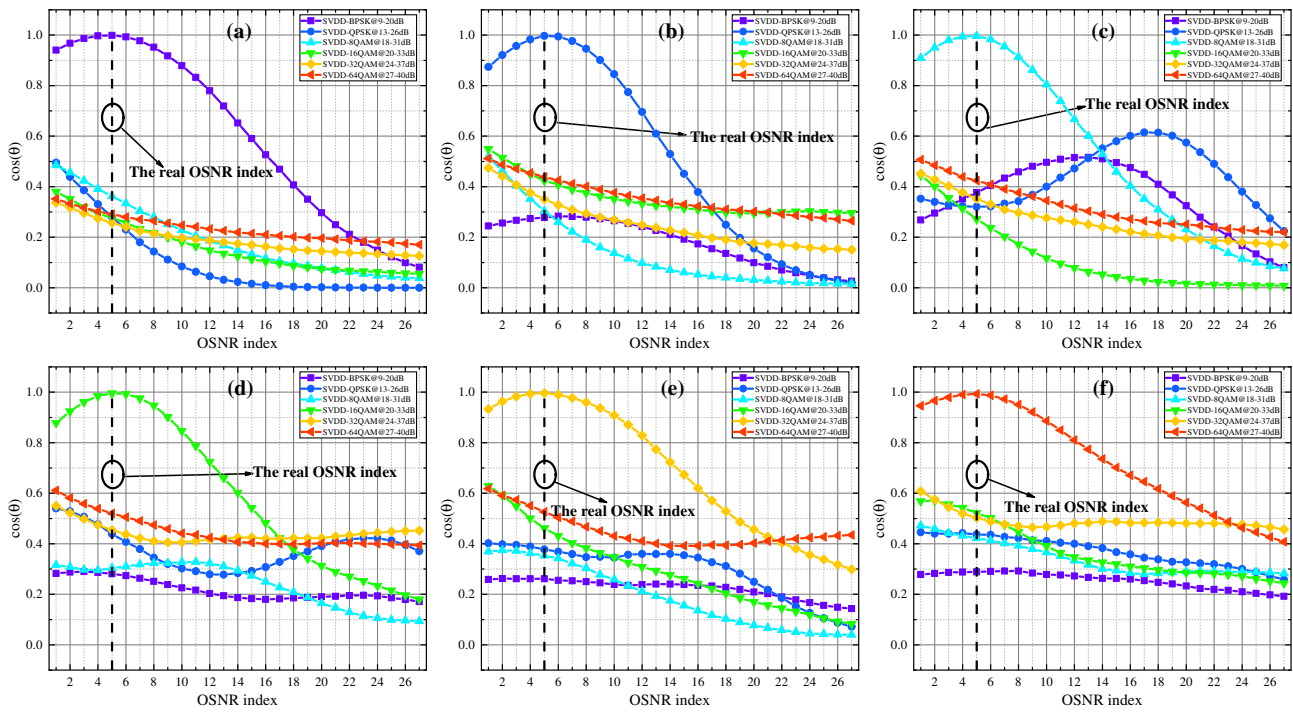


Fig. 3. $D(\mathbf{x}, \mathbf{s}_i)$ for (a) SVDD-BPSK, (b) SVDD-QPSK, (c) SVDD-8QAM, (d) SVDD-16QAM, (e) SVDD-32QAM, and (f) SVDD-64QAM with OSNR at corresponding 7% FEC threshold.

the cosine function of the acute angle between two vectors is also an effective metric of similarity [39], which can be written as follows:

$$D(\mathbf{x}, \mathbf{s}_i) = \cos(\theta_i) = \frac{\mathbf{x}^T \mathbf{s}_i}{\|\mathbf{x}\|_2 \|\mathbf{s}_i\|_2}, \quad (3)$$

where $\|\cdot\|_2$ denotes the l_2 -norm operation, and T denotes the transposition operation. If $\cos(\theta_i) > \cos(\theta_j), \forall j \neq i$, then the unknown pattern vectors are most similar to the sample pattern vectors \mathbf{s}_i . In this paper, the cosine similarity algorithm is employed to execute OPM, since the eigenvectors of signals with the same parameters have more similarity than different ones. Thus, we seek to tackle the OPM issue via searching the maximum cosine value between the eigenvector of the unknown signal and the eigenvectors of the sample signals. Figures 3(a) and 3(b) show the similarity of the six modulation formats (MFs) signals under their corresponding 7% forward error correction (FEC) threshold to the sample signals. Notice that the OSNR index in Figs. 3(a)-3(f) is obtained by numbering the corresponding OSNR intervals of different MFs selected in Section 3.A from the smallest value to the largest one. In other words, the same OSNR index with different MFs does not mean that the real OSNR is the same. It can be seen that the maximum similarity occurs under the condition that optical performance is the same between the unknown signal and the sample signals in the template base. This further proves that the trajectory information can be regarded as an ingenious option to carry out OPM.

3. SIMULATION AND ANALYSIS

The proposed joint numerical simulation system is constructed by utilizing MATLAB and VPI transmission Maker 9.3, as shown in Fig. 4. In the transmitter of this system, the continuous wave (CW) of the external cavity laser (ECL) with a linewidth of 100 kHz is split into X and Y polarization first by a polarization beam splitter (PBS) [40]. After that, the arbitrary waveform generator (AWG) outputs the radio frequency (RF) signals, which include 14/28 GBaud BPSK/QPSK/8QAM/16QAM/32QAM/64QAM. Note that the transmitted symbols are pulse shaped by a square root raised cosine (SRRC) finite impulse response (FIR) filter with a roll-off factor of 0.75. Then, they are loaded onto the X polarization of the lightwave via an in-phase quadrature (IQ) modulator, and the Y polarization is reserved as the optical carrier. A variable optical attenuator (VOA) is used to control the carrier to signal power ratio (CSPR) to 0 dB [5]. Both polarizations are then combined with a polarization beam combiner (PBC). It is worth mentioning that the launch power is optimized in this scheme under the short-range communication scenarios, i.e., setting the launch power to 2 dBm to achieve a trade-off between transmission performance and energy consumption [4]. To simulate various channel impairments, two specific modules are utilized in series in the transmission link. One module is the fiber, which can induce varying degrees of RCD by collaboratively setting its length and CD coefficients. The second module, which is composed of an amplified spontaneous emission (ASE) source and a VOA, is used to adjust the OSNR of the fiber link. In addition, an optical band pass filter (OBPF) with a bandwidth of 1.2 times baud rate is exploited to eliminate the outcome of band noise. At the receiving terminal, the Stokes vectors $S^r = [S_1^r, S_2^r, S_3^r]^T$

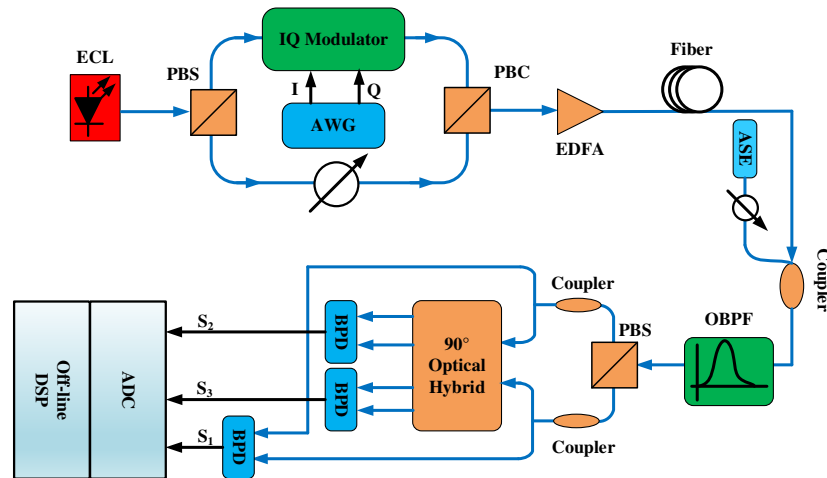


Fig. 4. Proposed joint numerical simulation system for SVDD.

are obtained by a SVR. Noting that, in the same transmission scenario, a total number of 32,768 symbols are obtained in each acquisition, and 50 independent data acquisitions are carried out by sweeping the random number seed.

In order to verify the effectiveness of the proposed OPM scheme in different scenarios, the following experiment is split into two subsections. In the first part, we will analyze both optimal parameters of the proposed scheme and the corresponding monitoring performance under joint MFI and OSNR monitoring scenarios. In the second one, we will utilize the proposed scheme to perform joint multi-parameter monitoring, including MFI, OSNR monitoring, and RCD estimation.

A. Optimization of Parameters and Joint MFI and OSNR Monitoring

By utilizing the simulation platform, as shown in Fig. 4, we acquired a large number of datasets for six commonly used MFs under different OSNR ranges, which were 9–22 dB for SVDD-BPSK, 13–26 dB for SVDD-QPSK, 18–31 dB for SVDD-8QAM, 20–33 dB for SVDD-16QAM, 24–37 dB for SVDD-32QAM, and 27–40 dB for SVDD-64QAM. Figure 5 illustrates their corresponding BERs under different OSNRs for these six kinds of MFs. It reveals that the OSNR values corresponding to 7% FEC thresholds ($\text{BER} = 3.8 \times 10^{-3}$) for SVDD-BPSK, SVDD-QPSK, SVDD-8QAM, SVDD-16QAM, SVDD-32QAM, and SVDD-64QAM are 10.8 dB, 14.7 dB, 19.5 dB, 22.2 dB, 25.8 dB, and 29.2 dB in this simulation system. It is evident that all of the selected OSNR ranges contain their corresponding 7% FEC thresholds; accordingly, the selected OSNR ranges are reasonable.

Considering the trade-off between accuracy and responsiveness, the number of used symbols is believed to be an important factor to evaluate the performance of the proposed scheme. In addition, based on the symmetry of the constellation about the origin, the folded operation is equivalent to a sharp increase of the number of symbols by four times compared with the un-folded operation. Accordingly, the influences of un-folded/folded operations and the number of used symbols are considered jointly in this study, where the number of mesh is

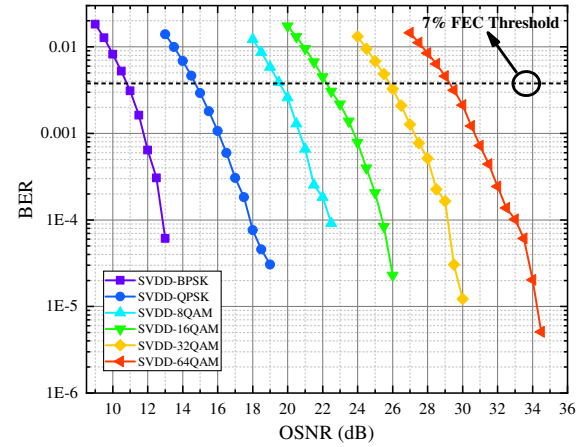


Fig. 5. Measured BER performance for different OSNR.

fixed at 10. Figure 6(a) depicts the average mean absolute error (MAE) of OSNR monitoring as a function of symbol numbers under un-folded/folded operations. The results demonstrate that the folded operation highly enhances the accuracy of OSNR monitoring compared with un-folded operations. Besides, we also observe that the performance of OSNR monitoring can be basically stabilized when the number of symbols is greater than 8192 under folded operations. Hence, in order to achieve optimistic OPM performance of the SVDD system, 8192 symbols and folded operations are applied in the following simulation tests.

Besides that, we also investigated the impact of mesh numbers on the performance of the proposed scheme. The average MAE of six MFs involved is calculated with different mesh numbers, as shown in Fig. 6(b). It can be found that under the mesh numbers are less, and the average MAE values decrease tempestuously if the number of meshes increases. Under the number of meshes greater than 10, the average MAE slightly fluctuates as the mesh numbers increase. Hence, we believe that the optimum number of meshes would be 10, with which the proposed scheme can achieve the best OPM performance. It is worth noting that all of the subsequent simulations are based

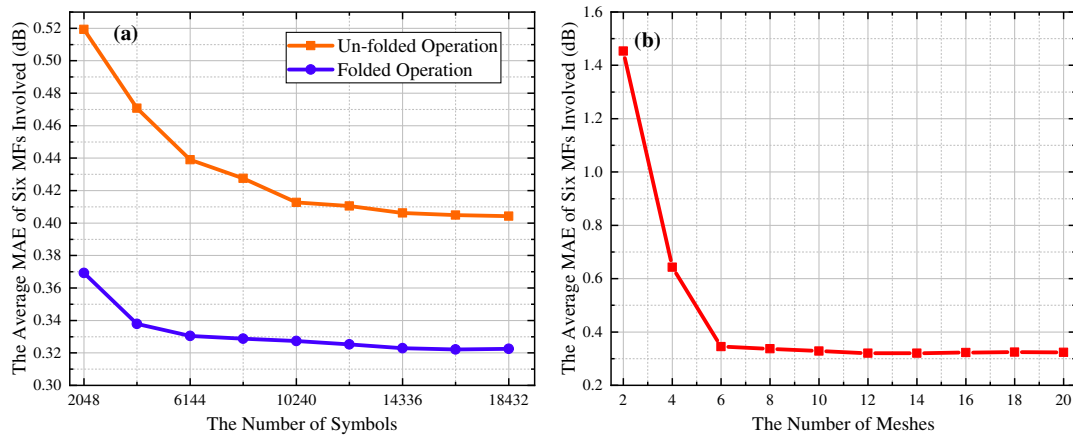


Fig. 6. (a) Average MAE of OSNR monitoring as a function of the number of symbols under the un-folded/folded operation and (b) the average MAE of OSNR monitoring as a function of the mesh numbers under the folded operation.

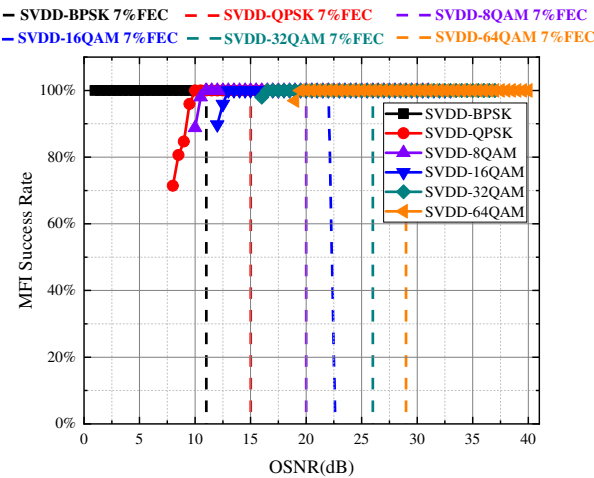


Fig. 7. MFI success rates with different OSNR conditions.

on the number of meshes derived from the experiments in our study.

Furthermore, Fig. 7 shows the MFI success rates under different OSNR conditions for those six MFs. Note here that in order to obtain the minimum OSNR required to achieve 100% successful recognition rate, we expand the selected reasonable OSNR described above. From the figure, we can conclude that the minimum OSNR required to achieve 100% MFI success rate is less than 1 dB, 10 dB, 11 dB, 13 dB, 16.5 dB, and 19.5 dB for SVDD-BPSK, SVDD-QPSK, SVDD-8QAM, SVDD-16QAM, SVDD-32QAM, and SVDD-64QAM, respectively, which is much smaller than the corresponding 7% FEC threshold. It reflects that the proposed scheme has excellent MFI performance. Moreover, this provides redundancy about reducing computational complexity for applications that only require MFI, as it can achieve just-right MFI performance by further reducing the number of meshes and symbols. The OSNR monitoring performances of these six MFs are depicted in Fig. 8. The blue dotted lines and the red dots denote the estimated OSNRs and the MAEs using the proposed scheme, respectively. It can be seen that the obtained OSNRs are in good agreement with the true OSNRs. Additionally, the average MAEs of estimated

OSNRs are 0.03 dB, 0.22 dB, 0.36 dB, 0.41 dB, 0.46 dB, and 0.49 dB for SVDD-BPSK, SVDD-QPSK, SVDD-8QAM, SVDD-16QAM, SVDD-32QAM, and SVDD-64QAM, respectively. That is to say, the accuracy of OSNR monitoring gradually decreases as the order of the MF increases. This may be due to the higher-order MF signals being more sensitive to ASE noise.

B. Multi-Parameter Optical Performance Monitoring

To explore multi-parameter OPM in our scheme, we append another optical parameter monitoring, i.e., RCD estimation, to further verify the trajectory information containing abundant optical parameter characteristics. The parameters used in this part are the optimal parameters discussed in Section 3.A. Besides, in order to verify the performance of multi-parameter OPM including MFI, OSNR monitoring, and RCD estimation by virtue of the proposed scheme, the detailed parameters for multi-parameter SVDD OPM are shown in Table 1. It can be found that they totally utilize 170,100 sets of data, including three kinds of MFs, 27 kinds of OSNR values, 21 kinds of RCD values, and 100 kinds of random number seed values. It should be noted that in these simulations three commonly used MFs are selected here, and similar results can be obtained for other types of MFs.

Figure 9 shows the MFI success rates under different OSNR and RCD values. The black dashed line represents the maximum tolerable RCD when the MFI rates are attained at 100% in all of the considered OSNR ranges. According to Fig. 9, it can be concluded that the SVDD-8QAM signal can be successfully identified 100% within the OSNR range of 18–31 dB and RCD of 0–200 ps/nm. For the SVDD-16QAM signal, it is identified as 100% within the range of 20–33 dB OSNR and 0–190 ps/nm RCD. The SVDD-32QAM signal can be 100% identified under conditions of 24–37 dB OSNR, whereas the tolerance of RCD is relatively poor, and the maximum tolerance to RCD is 0–160 ps/nm. In addition, as the order of the MF increases, the tolerances of the proposed scheme to ASE noise and RCD gradually decrease.

According to the above simulation results, in order to ensure that MFI rates maintain to the levels of 100%, the RCD range

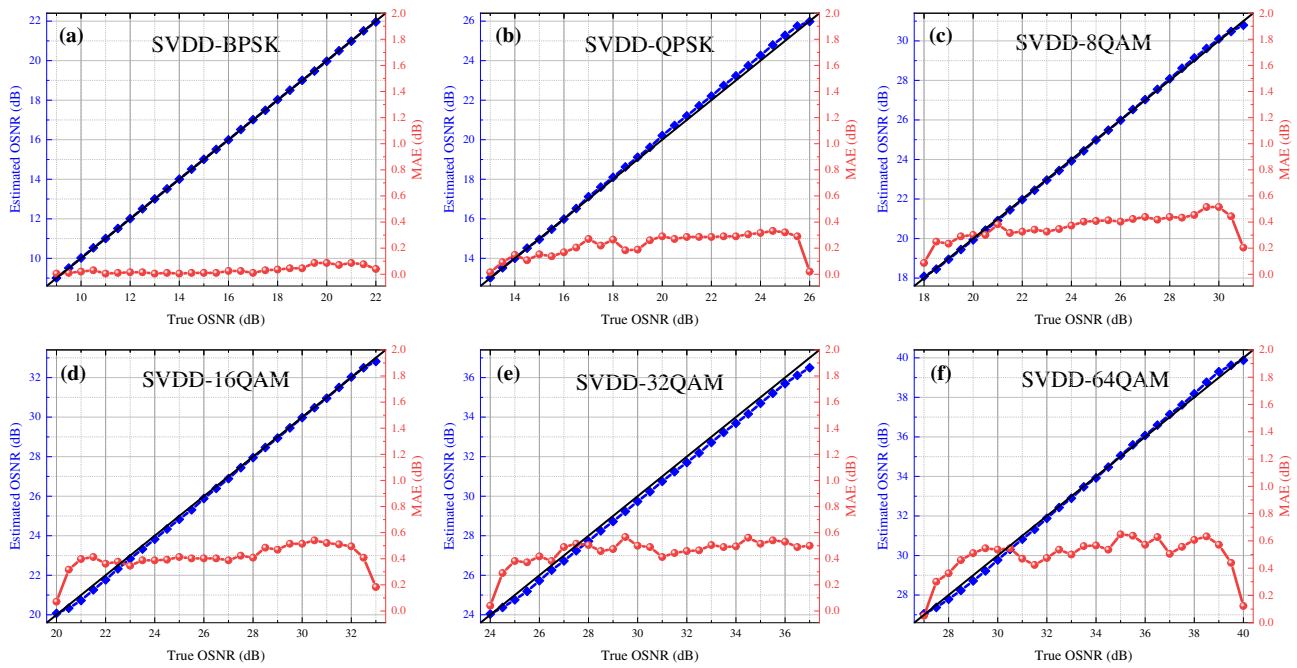


Fig. 8. OSNR monitoring performance for (a) SVDD-BPSK, (b) SVDD-QPSK, (c) SVDD-8QAM, (d) SVDD-16QAM, (e) SVDD-32QAM, and (f) SVDD-64QAM.

Table 1. Data Parameters for Multi-Parameter OPM for an SVDD System

| | SVDD-8QAM | SVDD-16QAM | SVDD-32QAM |
|------|----------------------|----------------------|----------------------|
| OSNR | 18–31 dB@0.5 dB | 20–33 dB@0.5 dB | 24–37 dB@0.5 dB |
| RCD | 0–200 ps/nm@10 ps/nm | 0–200 ps/nm@10 ps/nm | 0–200 ps/nm@10 ps/nm |

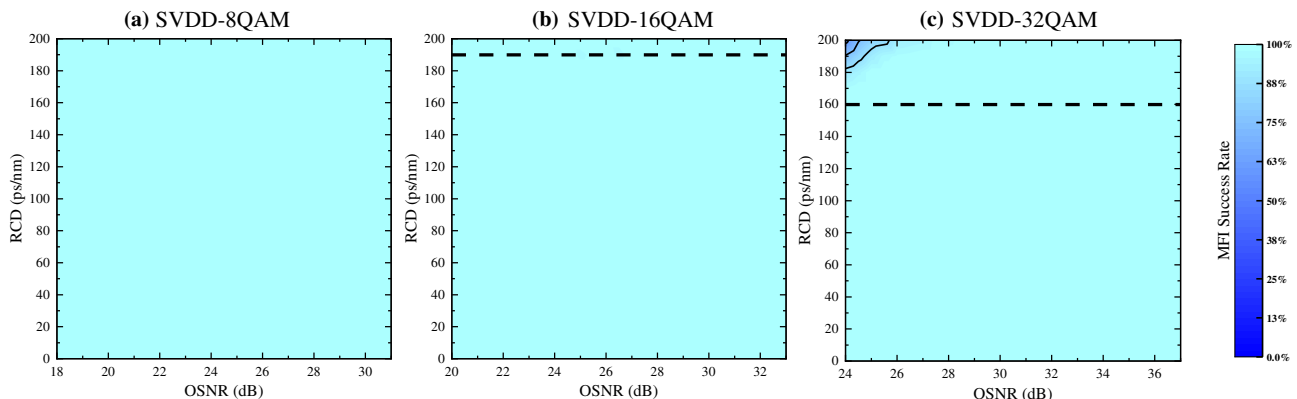


Fig. 9. MFI success rates under different OSNR and RCD values for (a) SVDD-8QAM, (b) SVDD-16QAM, and (c) SVDD-32QAM. The black dashed line represents the maximum tolerable RCD where the 100% MFI rates are attained in all of the considered OSNR ranges.

of 0–160 ps/nm is chosen to analyze the performance of the OSNR monitoring and RCD estimation using the proposed scheme. Figure 10(a) illustrates that the average MAEs of OSNR monitoring for SVDD-8QAM and SVDD-16QAM both remain within 1 dB when the RCD ranges are 0–160 ps/nm and 0–100 ps/nm, respectively. For SVDD-32QAM, the average MAE of OSNR monitoring can also stay around 2 dB when the RCD ranges are 0–130 ps/nm. Moreover, it is easy to find that following the increase of RCD, the OSNR monitoring errors gradually increase, which is due to severe deterioration of signal quality caused by the increase of RCD.

Figure 10(b) presents that the average MAE of the estimated RCD gradually decreases, which is benefited by the improvement of signal quality as the OSNR increases. In addition, the average MAE of the estimated RCD for these three selected MFs within the reasonable OSNR range considered are 2.82 ps/nm, 3.21 ps/nm, and 3.65 ps/nm, respectively. They are much smaller than the accumulation dispersion of optical pulse signals through 1 km standard single-mode fiber. Therefore, the proposed scheme can accurately estimate RCD. As a consequence, this module has the potential to be deployed in the DSP

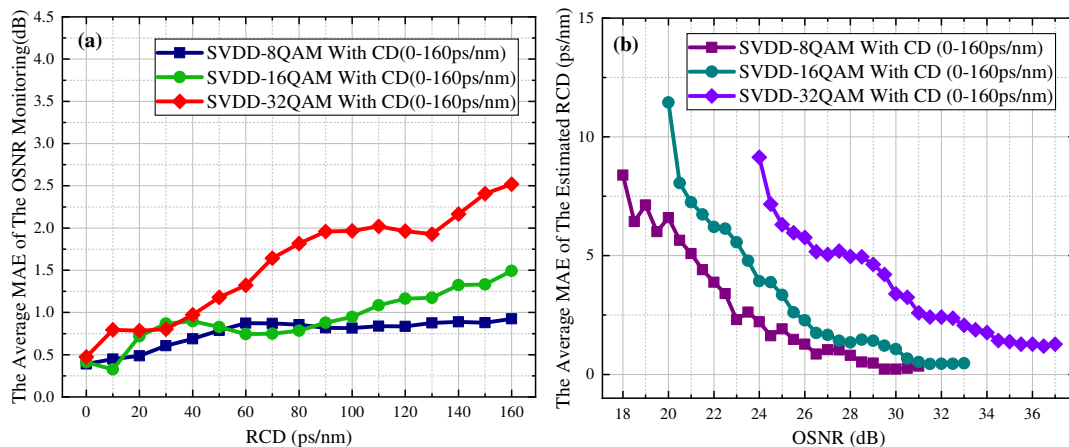


Fig. 10. (a) Average MAE of the OSNR monitoring versus RCD and (b) the average MAE of the estimated RCD versus OSNR.

module of the SVDD system for the short-reach communication network, which would greatly improve the compensation accuracy and self-adaptability of the CD compensation module.

4. PERFORMANCE EVALUATION

A. Robustness for Baud Rate

In order to verify the robustness of the proposed scheme to the baud rate, we select 14 GBaud signals as the reference for the 28 GBaud signals for performance comparison. It is interesting that all of the MFI success rates reach 100% for 14 GBaud SVDD-8QAM, SVDD-16QAM, and SVDD-32QAM signals, even if the RCD is as high as 200 ps/nm under the selected full ranges of OSNR. Figures 11(a) and 11(b) display the performance comparison of the OSNR monitoring and the estimated RCD in multi-parameter SVDD OPM for 14 GBaud and 28 GBaud signals, respectively. Note that the numerical labels in this picture represent the numerical value of the corresponding average MAE. In Fig. 11(a), we can see that the OSNR monitoring performance of the 14 GBaud signal is better than that of the 28 GBaud signal, and the monitoring errors are 0.7 dB, 0.5 dB, and 1 dB for SVDD-8QAM, SVDD-16QAM, and SVDD-32QAM, respectively. Those experimental characteristics are all

due to the greater tolerance of lower baud rate signals to noise values. However, from Fig. 11(b), we can easily obtain that the estimated MAE of the RCD for the 14 GBaud is 7 ps/nm higher than the 28 GBaud one. This may be due to the fact that lower baud rate signals tend to tolerate a greater degree of pulse broadening, which makes the dispersion differences of 10 ps/nm not have an obvious influence on the 14 GBaud signal over the 28 GBaud signal. Nonetheless, the estimation accuracy of the RCD by this scheme is also accurate, with estimation errors of 15 ps/nm, 10 ps/nm, and 6 ps/nm for the three commonly used MFs, respectively. Therefore, it can be concluded that the proposed scheme has strong robustness to the baud rate.

B. Computational Complexity

In this study, the computational complexity, as a key indicator to evaluate the performance of the proposed OPM scheme, is also examined with an insightful analysis. To consider the computational complexity of feature extraction and template matching, the pattern vectors of the sample signals are calculated and stored in memory in advance. The quantization of the trajectory information is completed using the received N symbols, where the weight coefficient matrix \mathbf{A} is constructed, and the computational complexity is recorded as $O(N)$. Letting

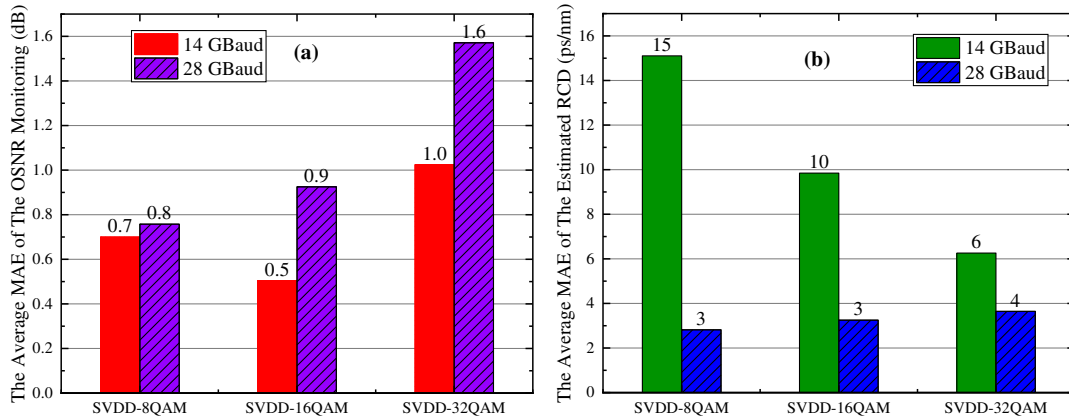


Fig. 11. Performance comparison of (a) the OSNR monitoring and (b) the estimated RCD in multi-parameter SVDD OPM for 14 GBaud and 28 GBaud signals.

Table 2. Performance Comparison between the Proposed Scheme and the Previous Schemes

| Type of Scheme | Monitored Parameters | Monitored Mode | Computation Complexity |
|-------------------------------|----------------------|----------------|------------------------|
| Proposed scheme | MF + OSNR + RCD | Joint | $O(N)$ |
| Density peak based [10] | MF | / | $O(N^2)$ |
| Density clustering based [35] | MF + OSNR | Joint | $O(N * \log N)$ |
| Godard's error based [36] | MF + CD + Nonlinear | Multi-stages | $O(N)$ |

$\gamma = M * M$ denote the total number of uniform meshes, the computational complexity of the obtained eigenvector related to the largest eigenvalue is $O(\gamma^2)$. At the template matching stage, the computational complexity for calculating the cosine value is $O(\gamma)$. Again, letting v be the number of the pattern vectors from sampled signals, which are stored in the template library, then the computational complexity for searching the maximum cosine value is denoted as $O(v \log v)$. As a consequence, the total computational complexity of the proposed OPM scheme is resulted as $O(N)$, since both γ and v are constants. As shown in Table 2, compared with other OPM monitoring methods [10,35], the OPM scheme based on trajectory information would present low complexity and more monitoring parameters. Furthermore, the proposed method implements joint rather than multi-stage multi-parameter OPM compared with the scheme [36]. Here, N in Table 2 represents the number of symbols used by the scheme.

In a nutshell, although the existing OPM scheme may also be applicable to the OPM of the SVDD system, to the best of our knowledge, the scheme that can jointly perform three-parameter OPM while requiring only low computational complexity is still lacking so far. This is important for SVDD optical transmission systems where computing resources are precious.

5. CONCLUSIONS

In this paper, we propose a joint multi-parameter OPM scheme with low complexity for the SVDD system by utilizing the trajectory information of the received signals for the first time, to the best of our knowledge. The effectiveness of the scheme has been verified by 14/28 GBaud SVDD-BPSK/-QPSK/-8QAM/-16QAM/-32QAM/-64QAM simulation systems. Under the scenario of joint MFI and OSNR monitoring, the identification rates of six MFs are completely 100% within the selected reasonable OSNR ranges. The average MAE values of the monitored OSNR are 0.03 dB, 0.22 dB, 0.36 dB, 0.41 dB, 0.46 dB, and 0.49 dB for 28 GBaud SVDD-BPSK/-QPSK/-8QAM/-16QAM/-32QAM/-64QAM signals, respectively. Under multi-parameter OPM scenarios, the proposed scheme can effectively identify SVDD-8QAM, SVDD-16QAM, and SVDD-32QAM, when RCDs are as high as 200 ps/nm, 190 ps/nm, and 160 ps/nm within the selected reasonable OSNR ranges. The average MAE of the OSNR monitoring and the estimated RCD for those MFs selected are 1.08 dB and 3.23 ps/nm, respectively. More interestingly, the proposed scheme shows strong robustness to the baud rates, and its overall computational complexity is $O(N)$. Thus, the proposed low-complexity trajectory-information-based OPM scheme for the SVDD system will have significant potential in applying

situations of short-reach optical communications broadly. Moreover, based on the rich difference characteristics contained in the trajectory information, the scheme has the potential to be applied to backbone optical networks and other linear and non-linear damage monitoring.

Funding. National Natural Science Foundation of China (61501213); Natural Science Foundation of Shandong Province (ZR2020MF012, ZR2020QF005); Liaocheng University (318051834, 318051835).

Disclosures. The authors declare no conflicts of interest.

Data Availability. Data underlying the results presented in this paper are not publicly available at this time but may be obtained from the authors upon reasonable request.

REFERENCES

- K. Zhong, X. Zhou, J. Huo, C. Yu, C. Lu, and A. P. T. Lau, "Digital signal processing for short-reach optical communications: a review of current technologies and future trends," *J. Lightwave Technol.* **36**, 377–400 (2018).
- M. Chagnon, "Optical communications for short reach," *J. Lightwave Technol.* **37**, 1779–1797 (2019).
- M. Chagnon, M. Morsy-Osman, and D. V. Plant, "Half-terabit single-carrier direct-detect transceiver, formats, and DSP: analysis and demonstration," *J. Lightwave Technol.* **36**, 447–459 (2018).
- D. Che, A. Li, X. Chen, Q. Hu, Y. Wang, and W. Shieh, "Stokes vector direct detection for short-reach optical communication," *Opt. Lett.* **39**, 3110–3113 (2014).
- D. Che and W. Shieh, "Polarization demultiplexing for Stokes vector direct detection," *J. Lightwave Technol.* **34**, 754–760 (2016).
- Y. Jin, D. Li, P. Yi, M. Cheng, S. Fu, M. Tang, D. Liu, and L. Deng, "Adaptive blind Stokes-space based equalizer for RSOP in SV-DD systems with high chromatic dispersion tolerance," *IEEE Photon. J.* **12**, 7200913 (2020).
- N. Cui, Z. Zheng, X. Zhang, W. Yi, R. Guo, W. Zhang, X. Tang, H. Xu, and L. Xi, "Joint blind equalization of CD and RSOP using a time-frequency domain Kalman filter structure in Stokes vector direct detection system," *Opt. Express* **27**, 11557–11570 (2019).
- Z. Dong, F. N. Khan, Q. Sui, K. Zhong, C. Lu, and A. P. T. Lau, "Optical performance monitoring: a review of current and future technologies," *J. Lightwave Technol.* **34**, 525–543 (2016).
- Z. Wan, Z. Yu, L. Shu, Y. Zhao, H. Zhang, and K. Xu, "Intelligent optical performance monitor using multi-task learning based artificial neural network," *Opt. Express* **27**, 11281–11291 (2019).
- L. Jiang, L. Yan, A. Yi, Y. Pan, T. Bo, M. Hao, W. Pan, and B. Luo, "Blind density-peak-based modulation format identification for elastic optical networks," *J. Lightwave Technol.* **36**, 2850–2858 (2018).
- L. Jiang, L. Yan, A. Yi, Y. Pan, M. Hao, W. Pan, and B. Luo, "An effective modulation format identification based on intensity profile features for digital coherent receivers," *J. Lightwave Technol.* **37**, 5067–5075 (2019).
- L. Lundberg, H. Sunnerud, and P. Johannesson, "In-band OSNR monitoring of PM-QPSK using the Stokes parameters," in *Optical Fiber Communication Conference* (Optical Society of America, 2015), paper W4D.5.
- F. N. Khan, K. Zhong, W. H. Al-Arashi, C. Yu, C. Lu, and A. P. T. Lau, "Modulation format identification in coherent receivers using deep

- machine learning," *IEEE Photon. Technol. Lett.* **28**, 1886–1889 (2016).
- 14. S. M. Ranzini, F. Da Ros, H. Bülow, and D. Zibar, "Tunable optoelectronic chromatic dispersion compensation based on machine learning for short-reach transmission," *Appl. Sci.* **9**, 4332 (2019).
 - 15. M. Hao, L. Yan, A. Yi, L. Jiang, Y. Pan, W. Pan, and B. Luo, "OSNR monitoring using support vector ordinal regression for digital coherent receivers," *IEEE Photon. J.* **11**, 7906611 (2019).
 - 16. J. Li, D. Wang, and M. Zhang, "Low-complexity adaptive chromatic dispersion estimation scheme using machine learning for coherent long-reach passive optical networks," *IEEE Photon. J.* **11**, 7905711 (2019).
 - 17. S. Guo, P. Guo, A. Yang, and Y. Qiao, "Deep neural network based chromatic dispersion estimation with ultra-low sampling rate for optical fiber communication systems," *IEEE Access* **7**, 84155–84162 (2019).
 - 18. X. Yu, C. Bai, H. Xu, W. Sun, L. Yang, H. Zheng, and W. Hu, "A modified PSO assisted blind modulation format identification scheme for elastic optical networks," *Opt. Commun.* **476**, 126280 (2020).
 - 19. R. Zhao, W. Sun, H. Xu, C. Bai, X. Tang, Z. Wang, L. Yang, L. Cao, Y. Bi, X. Yu, W. Fang, B. Li, T. Zhou, and P. Ge, "Blind modulation format identification based on improved PSO clustering in a 2D Stokes plane," *Appl. Opt.* **60**, 9933–9942 (2021).
 - 20. S. Fu, Z. Xu, J. Lu, H. Jiang, Q. Wu, Z. Hu, M. Tang, D. Liu, and C. C.-K. Chan, "Modulation format identification enabled by the digital frequency-offset loading technique for hitless coherent transceiver," *Opt. Express* **26**, 7288–7296 (2018).
 - 21. M. Xiang, Q. Zhuge, M. Qiu, X. Zhou, M. Tang, D. Liu, S. Fu, and D. V. Plant, "RF-pilot aided modulation format identification for hitless coherent transceiver," *Opt. Express* **25**, 463–471 (2017).
 - 22. C. Zhu, A. V. Tran, S. Chen, L. B. Du, C. C. Do, T. Anderson, A. J. Lowery, and E. Skafidas, "Statistical moments-based OSNR monitoring for coherent optical systems," *Opt. Express* **20**, 17711–17721 (2012).
 - 23. H. Xu, L. Yang, X. Yu, Z. Zheng, C. Bai, W. Sun, and X. Zhang, "Blind and low-complexity modulation format identification scheme using principal component analysis of Stokes parameters for elastic optical networks," *Opt. Express* **28**, 20249–20263 (2020).
 - 24. Y. Ma, M. Gao, L. Wang, Y. Sha, W. Shao, and G. Shen, "Accuracy enhancement of moments-based OSNR monitoring in QAM coherent optical communication," *IEEE Commun. Lett.* **24**, 821–824 (2020).
 - 25. D. Tang, X. Wang, L. Zhuang, P. Guo, A. Yang, and Y. Qiao, "Delay-tap-sampling-based chromatic dispersion estimation method with ultra-low sampling rate for optical fiber communication systems," *IEEE Access* **8**, 101004 (2020).
 - 26. D. Wang, M. Wang, M. Zhang, Z. Zhang, H. Yang, J. Li, J. Li, and X. Chen, "Cost-effective and data size adaptive OPM at intermediated node using convolutional neural network-based image processor," *Opt. Express* **27**, 9403–9419 (2019).
 - 27. Z. Wang, A. Yang, P. Guo, and P. He, "OSNR and nonlinear noise power estimation for optical fiber communication systems using LSTM based deep learning technique," *Opt. Express* **26**, 21346–21357 (2018).
 - 28. Y. Zhao, Z. Yu, Z. Wan, S. Hu, L. Shu, J. Zhang, and K. Xu, "Low complexity OSNR monitoring and modulation format identification based on binarized neural networks," *J. Lightwave Technol.* **38**, 1314–1322 (2020).
 - 29. T. Tanimura, T. Hoshida, T. Kato, S. Watanabe, and H. Morikawa, "Convolutional neural network-based optical performance monitoring for optical transport networks," *J. Opt. Commun. Netw.* **11**, A52–59 (2019).
 - 30. A. Yi, L. Yan, H. Liu, L. Jiang, Y. Pan, B. Luo, and W. Pan, "Modulation format identification and OSNR monitoring using density distributions in Stokes axes for digital coherent receivers," *Opt. Express* **27**, 4471–4479 (2019).
 - 31. Y. Cheng, S. Fu, M. Tang, and D. Liu, "Multi-task deep neural network (MT-DNN) enabled optical performance monitoring from directly detected PDM-QAM signals," *Opt. Express* **27**, 19062–19074 (2019).
 - 32. X. Fan, L. Wang, F. Ren, Y. Xie, X. Lu, Y. Zhang, T. Zhangsun, W. Chen, and J. Wang, "Feature fusion-based multi-task ConvNet for simultaneous optical performance monitoring and bit-rate/modulation format identification," *IEEE Access* **7**, 126709 (2019).
 - 33. W. S. Saif, T. Alshawi, M. A. Esmail, A. Ragheb, and S. Alshebeili, "Separability of histogram based features for optical performance monitoring: an investigation using t-SNE technique," *IEEE Photon. J.* **11**, 7203012 (2019).
 - 34. M. C. Tan, F. N. Khan, W. H. Al-Arashi, Y. Zhou, and A. P. Tao Lau, "Simultaneous optical performance monitoring and modulation format/bit-rate identification using principal component analysis," *J. Opt. Commun. Netw.* **6**, 441–448 (2014).
 - 35. Z. Zhao, A. Yang, P. Guo, and Q. Tan, "A density clustering algorithm for simultaneous modulation format identification and OSNR estimation," *Appl. Sci.* **10**, 1095 (2020).
 - 36. L. Jiang, L. Yan, A. Yi, Y. Pan, M. Hao, W. Pan, B. Luo, and Y. Jaouën, "Chromatic dispersion, nonlinear parameter, and modulation format monitoring based on Godard's error for coherent optical transmission systems," *IEEE Photon. J.* **10**, 7900512 (2018).
 - 37. C. Xie, "Chromatic dispersion estimation for single-carrier coherent optical communications," *IEEE Photon. Technol. Lett.* **25**, 992–995 (2013).
 - 38. K. S. Trivedi, "Discrete-time Markov chains," in *Probability and Statistics with Reliability, Queuing and Computer Science Applications* (John Wiley & Sons, 2016), pp. 351–419.
 - 39. X.-D. Zhang, *Matrix Analysis and Applications* (Cambridge University, 2017).
 - 40. T. M. Hoang, Q. Zhuge, Z. Xing, M. Sowailem, M. Morsy-Osman, and D. V. Plant, "Single wavelength 480 Gb/s direct detection transmission over 80 km SSMF enabled by Stokes vector receiver and reduced-complexity SSBI cancellation," in *Optical Fiber Communications Conference and Exposition (OFC)* (2018), pp. 1–3.